

**The development and evaluation of airborne in situ N₂O
and CH₄ sampling using a Quantum Cascade Laser
Absorption Spectrometer (QCLAS)**

**J. R. Pitt¹, M. le Breton¹, G. Allen¹, C. J. Percival¹, M. W. Gallagher¹, S. J.-B.
Bauguitte², S. J. O'Shea¹, J. B. A. Muller^{1*}, M. S. Zahniser³, J. Pyle⁴, P.I. Palmer⁵**

[1]{School of Earth, Atmospheric and Environmental Sciences, University of Manchester,
Oxford Road, Manchester, M13 9PL, UK}

[2]{Facility for Airborne Atmospheric Measurements (FAAM), Building 125, Cranfield
University, Cranfield, Bedford, MK43 0AL, UK}

[3]{Aerodyne Research, Inc., Center for Atmospheric and Environmental Chemistry,
Billerica, Massachusetts, USA}

[4]{Centre for Atmospheric Science, University of Cambridge, Cambridge CB2 1EW, UK}

[5]{School of GeoSciences, The University of Edinburgh, Edinburgh, EH9 3JN, UK}

[*]{now at: Deutscher Wetterdienst, Meteorologisches Observatorium Hohenpeißenberg,
Germany}

Correspondence to: J. R. Pitt (joseph.pitt@manchester.ac.uk)

1 Abstract

2 Spectroscopic measurements of atmospheric N₂O and CH₄ mole fractions were made on
3 board the FAAM (Facility for Airborne Atmospheric Measurements) large Atmospheric
4 Research Aircraft. We present details of the mid-IR ~~Aerodyne Research Inc.~~ Quantum
5 Cascade Laser Absorption Spectrometer (QCLAS, Aerodyne Research Inc., USA) employed,
6 including its configuration for airborne sampling, and evaluate its performance over 17 flights
7 conducted during summer 2014. Two different methods of correcting for the influence of
8 water vapour on the spectroscopic retrievals are compared and evaluated. A new in-flight
9 calibration procedure to account for the observed sensitivity of the instrument to ambient
10 pressure changes is described, and its impact on instrument performance is assessed. Test
11 flight data linking this sensitivity to changes in cabin pressure is presented. Total 1 σ
12 uncertainties of ~~2.471-81~~ ppb for CH₄ and ~~0.540-35~~ ppb for N₂O are derived. We report a
13 mean difference in 1 Hz CH₄ mole fraction of 2.05 ppb (1 σ = 5.85 ppb) between in-flight
14 measurements made using the QCLAS and simultaneous measurements using a previously
15 characterised ~~Los Gatos Research~~ Fast Greenhouse Gas Analyser (FGGA, Los Gatos
16 Research, USA). Finally, a potential case study for the estimation of a regional N₂O flux
17 using a mass balance technique is identified, and the method for calculating such an estimate
18 is outlined.

1. Introduction

CH₄ and N₂O emissions together comprise 38% of the total global radiative forcing attributable to emissions of well-mixed greenhouse gases (Myhre et al., 2013). N₂O is also a major component of stratospheric chemical cycles, acting as the largest contributing species towards stratospheric ozone depletion, and predicted to remain so throughout the 21st century (Ravishankara et al., 2007). CH₄ emissions can also lead to the formation of tropospheric ozone through reaction with OH radicals, leading to air quality issues associated with potentially dangerous respiratory problems in many cities across the world (Ebi and McGregor, 2008).

The globally averaged atmospheric abundances of CH₄ and N₂O have increased respectively from 722 ± 25 ppb to 1803 ± 2 ppb and 270 ± 7 ppb to 324.2 ± 0.2 ppb in the period 1750 to 2011 (Hartmann et al., 2013). However, the relative contribution of individual sources and sinks to the atmospheric abundance of both species is highly uncertain (Ciais et al., 2013; Kirschke et al., 2013). Top-down, [atmospheric](#) measurement based approaches can provide important constraints on these global budgets, both through direct estimation of sectorally and/or regionally disaggregated emissions using atmospheric inversion models (Fraser et al., 2013; Thompson et al., 2014), and by enabling validation of the process models used to compile bottom-up emission inventories (Krinner et al., 2005; O'Shea et al., 2014b). Representative sampling on regional and national scales can also act as an important aid to establishing effective emission reduction policies at both national and international levels.

In situ aircraft-based measurements form an important part of this top-down approach, enabling high-resolution sampling on regional scales (e.g. O'Shea et al., 2013a), vertical profile measurement (e.g. Wofsy et al., 2011), and sampling in remote regions far from ground stations (e.g. Kort et al., 2012). Greenhouse gas flux estimates can then be made using mass balance (Karion et al., 2013; O'Shea et al., 2014a; Peischl et al., 2015), eddy covariance (Ritter et al., 1992; Hiller et al., 2014; Yuan et al., 2015) or inverse modelling techniques (Kort et al., 2008; Polson et al., 2011; Xiang et al., 2013), the latter frequently in association with ground-based measurements (Miller et al., 2013). Aircraft measurements can also be used to validate both ground-based and satellite-based remote sensing techniques, forming an important link across a wide range of spatial and temporal measurement scales (Tanaka et al., 2012; Wecht et al., 2012). [However, it should be noted that of the studies listed above, only Wofsy et al. \(2011\) and Xiang et al. \(2013\) made continuous in situ measurements of N₂O.](#)

emphasising the need for wider deployment of in situ instrumentation to measure N₂O on aircraft.

During summer 2014, the FAAM (Facility for Airborne Atmospheric Measurements) large Atmospheric Research Aircraft (hereafter referred to as the FAAM aircraft) participated in the GAUGE (Greenhouse gAs UK and Global Emissions) and MAMM (Methane and other greenhouse gases in the Arctic: Measurements, process studies and Modelling) measurement campaigns. This aircraft component of the GAUGE campaign focussed on greenhouse gas measurement around the UK, to allow emission estimates to be made in conjunction with both inverse modelling and mass balance techniques. An important element of this campaign was to better constrain emissions from the agricultural sector, which is the second largest contributor (after the energy sector) towards the UK's total greenhouse gas emissions, producing N₂O through the use of nitrogen-based fertilisers and CH₄ by enteric fermentation in livestock (Webb et al., 2014). The MAMM campaign focussed on improving understanding of Arctic CH₄ emissions, dominated by biogenic emission from natural wetlands (Zhuang et al., 2006), in order to help better constrain measurement-derived global CH₄ budgets and to allow comparison against the emissions predicted by regional land surface models (O'Shea et al., 2014b). Accurate measurement of CH₄ and N₂O on board the FAAM aircraft was therefore of critical importance during these campaigns.

Infrared (IR) spectroscopy is frequently employed for airborne measurement of greenhouse gas mole fractions (Chen et al., 2010; O'Shea et al., 2013b; Santoni et al., 2014), enabling high frequency measurement (usually ≥ 1 Hz) and ~~small-fast~~ instrument response times (of the order seconds). Many instruments make use of the superior lasers, optics and detectors available ~~at near-IR wavenumbers of~~ in the near-IR region around $\sim 6000\text{ cm}^{-1}$ (Baer et al., 2002; Crosson, 2008). However, line strengths for CH₄ and N₂O are of the order 100 and 100,000 times stronger respectively in the mid-IR spectral region of $\sim 1000\text{--}4000\text{ cm}^{-1}$ (Rothman et al., 2013). For CH₄ these competing effects lead instruments operating in both spectral ranges to achieve broadly comparable performances. For N₂O, however, the comparatively weak line strengths in the near-IR, coupled with the lower atmospheric abundance of N₂O, make mid-IR spectroscopy much more suitable for atmospheric measurement. Rannik et al. (2015) find that the best long-term and short-term precisions for N₂O measurement are obtained using continuous-wave quantum cascade laser (QCL) based instruments, which operate in the mid-IR region.

1 In this paper we discuss the development of an airborne measurement system for CH₄ and
2 N₂O, using a mid-IR, continuous-wave, ~~Aerodyne Research Inc.~~ Quantum Cascade Laser
3 Absorption Spectrometer (QCLAS, ~~Aerodyne Research Inc., USA~~) on board the FAAM
4 aircraft. We focus on measurements from the GAUGE and MAMM campaigns conducted
5 during summer 2014.

6 Details of the direct absorption spectroscopy and associated spectral retrieval algorithm
7 employed are given in Sect. 2, including the empirically derived correction for the presence of
8 water vapour. The configuration and optimisation of the sample and calibration air flow
9 systems for airborne measurement are also presented in this section. In Sect. 3, calibration
10 procedures used to tie the data to the WMO (World Meteorological Office) greenhouse gas
11 scale are described and assessed, both through analysis of in-flight calibration data and
12 comparison with simultaneous CH₄ measurements using a ~~Los Gatos Research~~ Fast
13 Greenhouse Gas Analyser (FGGA, Model RMT-200, ~~Los Gatos Research, USA~~; described by
14 O'Shea et al., 2013b). Section 4 presents N₂O data from GAUGE flight B868 in more detail,
15 and outlines how this data could be used in combination with a mass balance technique to
16 estimate a regional N₂O flux for the northwest of England. Finally, the key findings of this
17 work are summarised in Sect. 5.

19 2. Operational Design

20 2.1 Instrument Specification

21 In this section we briefly describe the operating principles of the ~~QCLAS Aerodyne Research~~
22 ~~Inc. Quantum Cascade Laser Mini-Monitor~~ used to measure N₂O and CH₄ on board the
23 FAAM aircraft. This instrument uses a mid-IR, thermoelectrically cooled, continuous-wave,
24 distributed feedback QCL (Alpes Laser, Switzerland) as a light source. The laser beam is
25 directed through an astigmatic Herriott multipass absorption cell, providing an effective
26 optical pathlength through the sample of 76 m (McManus et al., 1995), and collected by a
27 thermoelectrically cooled photovoltaic detector (Vigo Systems, Poland). The output
28 frequency of the QCL is scanned over a small spectral region (1275.3–1275.8 cm⁻¹),
29 containing ro-vibrational N₂O, CH₄ and H₂O line transitions, by repeatedly ramping the laser
30 current whilst holding the laser at a constant temperature. The laser is swept across this region
31 at a rate of ~ 5 kHz, with a measurement of the detector's zero-light output (noise-equivalent-
32 signal) recorded at the end of each sweep by dropping the current below the laser threshold

(such that there is no emission from the laser). Because the linear current ramp does not produce a precisely linear frequency response from the laser, it is necessary to determine the tuning rate using a Germanium etalon, which can be placed in the path of the beam before the multipass cell.

The laser temperature is held at $\sim -23\text{ }^{\circ}\text{C}$ using a Peltier cooler. Excess heat is removed using a coolant fluid, which is recirculated and maintained at $\sim 25\text{ }^{\circ}\text{C}$ by a CustomChill thermoelectric liquid chiller (CRAL300DHP-12; CustomChill, USA). The optical layout of the instrument is described in detail by Nelson et al. (2004), although our use here of a continuous-wave laser rather than a pulsed laser allows for removal of the beamsplitter and the incorporation of two additional mirrors to aid the adjustment of beam alignment prior to entering the cell.

2.2 TDLWintel Software

The laser current control and mole fraction retrievals were performed using the TDLWintel software package, details of which are provided by Nelson et al. (2002). In brief, this retrieval relies on the Beer-Lambert law, given by;

$$\frac{I(\nu)}{I_0(\nu)} = \exp(-\alpha(\nu, P, T)nCl) \quad (1)$$

where l is the path length of the beam through the absorber, C is the concentration of sample gas, n is the absorber mole fraction and $\alpha(\nu, P, T)$ is the frequency, pressure and temperature dependent absorption cross section of the absorber. The intensity $I(\nu)$ is measured by the detector, which also measures the background intensity $I_0(\nu)$ at window wavelengths outside the wings of target absorption lines. A polynomial fit is applied to the data obtained at these non-absorbing wavelengths such that variation in baseline intensity measurement, due to changes in both laser output and detector sensitivity across the measured spectral range, can be subtracted from the spectrum (Zahniser et al., 1995).

In order to determine the mole fraction of a target species at a sampling rate of 1 Hz, TDLWintel fits a Voigt line shape profile to an averaged spectrum, consisting of ~ 5000 individual laser sweeps, using a Levenberg-Marquardt retrieval algorithm. Line strengths and positions are taken from the HITRAN 2012 database (Rothman et al., 2013). The pressure and temperature of the sample are continuously measured by in situ sensors positioned within the

sample gas flow on the outlet of the cell, allowing air broadening effects to be considered in the retrieval.

2.3 Configuration for Airborne Measurement

The QCLAS is mounted on a rack inside the cabin of the FAAM aircraft, with a rearward facing, 3/8" outer diameter, stainless steel inlet inserted through a customised window blank (Avalon Aero Ltd., UK). The sample flow line consists of Swagelok 1/4" outer diameter PFA Teflon tubing, partly encased within the inlet, and forming a pressure seal via a bored-through Swagelok 3/8" to 1/4" reducing union. Figure 1 shows a schematic of the QCLAS air sampling system including the configuration for delivering calibration gas to the sample cell. The sample flow line is ~ 2.5 m in length from the inlet tip to the pressure controller. Sample flow rate is measured using a 30 SLPM (Standard Litres Per Minute) mass flow meter (M10MB01334CS3BV, MKS Instruments UK Ltd, UK), placed directly upstream of a 0.5 μ m sintered particle filter (SS-4F-05, Swagelok, USA).

The choice of sample cell pressure is a balance between two effects: higher pressures increase the absorption, thus improving the signal-to-noise ratio of the measurement, whilst pressure broadening of the spectral lines increases spectral overlap and line mixing (as discussed by Zahniser et al., 1995). Airborne operation is also complicated by the large variation in inlet pressures typically encountered over the course of a flight (down to ~ 250 hPa at 10 km altitude).

Control of the cell pressure is provided by an electronic pressure controller (640A-13TS1V62V, MKS Instruments UK Ltd, UK) placed upstream of the sample cell, as shown in Fig. 1. This maintains a constant pressure by automatically adjusting an internal valve to restrict the flow of air through it. As the inlet pressure decreases, the valve is set to a progressively more open position. The minimum inlet pressure that can be sampled whilst maintaining any given cell pressure is attained when the pressure controller valve reaches its fully open position. This minimum inlet pressure is then equal to the sum of the (chosen) cell pressure and the pressure drops across each component of the inlet system (including the fully open pressure controller valve). Hence choosing a lower cell pressure decreases this minimum inlet pressure, enabling the cell to be held at constant pressure up to a higher altitude. A cell pressure of 68.9 ± 3.6 hPa (at 1σ) was used during the GAUGE and MAMM campaigns.

Air is pulled through the system using a single stage scroll pump (Edwards XDS10, Edwards, UK). A throttle valve (253B-1-40-1, MKS Instruments UK Ltd, UK) positioned between the

sample cell outlet and the pump inlet is used to control the flow rate through the system. This again is a balance between the desire to decrease the instrument response time, favouring a faster flow rate, and the desire to reduce the total pressure drop between the inlet and the sample cell, favouring a slower flow rate. Throughout the GAUGE and MAMM campaigns the valve was set to 18% of its fully open position, resulting in a constant mass flow rate of 1.43 ± 0.21 SLPM (at 1σ) down to inlet pressures of ~ 380 hPa. At lower inlet pressures both the mass flow rate and the cell pressure were reduced.

Laboratory tests were performed to establish the effect of cell pressure changes on the mole fractions retrieved when sampling a compressed air cylinder. The variability in retrieved mole fraction was found to be no greater across cell pressures typically encountered during high altitude flying (inlet pressures below 380 hPa; cell pressures down to ~ 46 hPa) than across the range experienced during low altitude flying (inlet pressures above 380 hPa; cell pressures between 65 hPa and 76 hPa). It was therefore deemed unnecessary to filter data according to the absolute cell pressure value. However, rapid changes in pressure were found to impact upon the retrieved mole fractions; consequently data was removed whenever the 10 s standard deviation in cell pressure exceeded 0.1 Torr (13.3 Pa).

The response time of the system was determined in the laboratory (at 1017 hPa inlet pressure) by overflowing the inlet with N_2 from a compressed gas cylinder. The e-folding time of the system was determined using an exponential fit to the decay in retrieved mole fractions, and was found to be 0.68 ± 0.12 s (mean $\pm 1\sigma$). The inlet lag time was given by the time between turning on the N_2 flow and the first drop in retrieved mole fractions. In this laboratory test it was found to be in the range 2–3 seconds; however, we expect this lag time to decrease with altitude (up to ~ 380 hPa) as the volumetric flow rate of the system scales inversely with air density (for a constant mass flow rate).

In principle the Beer-Lambert relationship described above can be used to retrieve absolute mole fractions. However, in-flight calibration is commonly used to account for instrumental drift when using optical-based measurements (e.g. O'Shea et al., 2013b; Santoni et al., 2014), as external variables such as temperature and pressure can undergo significant variation during a flight. Our system employs three calibration standards to scale the data and assess instrument performance, as described in Sect. 3.1.

The 3 calibration standards are stored in 10 L carbon fibre hoop-wrap cylinders (BFC 124-136-002, Aluminium Alloy 7060, Luxfer, UK), which are filled to ~ 300 bar and mounted to

the QCLAS rack. Each cylinder is fitted with a high pressure brass valve (C215, Rotarex, Luxembourg), screwed into the cylinder collar using PTFE (polytetrafluoroethylene) tape. An all brass adapter connects this to instrument-grade stainless steel tubing of 1/8" outer diameter, specially cleaned for high purity service (21512, Thames-Restek, UK). This tube joins each cylinder to a separate single-stage diaphragm brass regulator (44-2212-244-1382, TESCO, UK). On the low pressure side of the regulator Swagelok 1/8" outer diameter PFA Teflon tubing is used. Three 3-way valves (009-0294-900, Parker-Hannifin, USA) and one 2-way valve (009-0089-900, Parker-Hannifin, USA) are used to select the flow from the desired calibration cylinder (a fourth port allows sampling from an external cylinder). The flow rate is set using a mass flow controller (1179A01314CS1BV, MKS Instruments UK Ltd, UK) to provide an overflow of calibrant at the inlet (upstream of the mass flow meter).

2.4 Water Vapour Correction

The influence of water vapour on spectral retrievals can be very significant (e.g. Allen et al., 2014), particularly given the wide range of natural water vapour concentrations typically encountered over the course of a flight (from a small fraction of a percent to many percent in the troposphere alone). To ensure comparability between measurements made at different humidity levels it is necessary to remove this effect and report dry mole fractions.

Many opt to circumvent the need to correct for this influence by drying the sample air before it enters the instrument, often using a combination of Nafion gas dryers and dry ice traps (e.g. Daube et al., 2002; Peischl et al., 2010; Santoni et al., 2014). The advantage of this approach is obvious, as any empirically derived correction for the influence of water vapour will contribute, often significantly, to the overall uncertainty of the measurements. However, there are several disadvantages associated with drying the sample, as discussed in detail by Rella et al. (2013). Of particular relevance for the QCLAS system described here are the issues associated with increasing the pressure drop across the inlet system, increasing the residence time in the inlet system, and the logistical problems of supplying dry ice to remote field locations and transporting it in a sealed cabin environment.

In cases such as this, where the sample is not dried, an empirical correction must be derived in order to account for the water vapour influence. Typically this involves applying a scale factor to the retrieved mole fractions, with its form and coefficients determined through laboratory experiment. Rella et al. (2013), O'Shea et al. (2013b) and Zellweger et al. (2012) employ this approach across a variety of spectroscopic instruments. However, a recently added feature of

the TDLWintel software allows the effect of line broadening (in addition to sample dilution) due to the presence of water vapour to be included in the spectroscopic retrieval itself. Instrument-specific ~~ratios-coefficients~~ quantifying the broadening due to water vapour ~~in terms of the broadening due to air~~ must be derived empirically for each species. These coefficients are equal to the dimensionless ratio of the line broadening due to water vapour pressure to the line broadening due to dry air pressure. Water corrected mole fractions are then determined by first retrieving the water vapour mole fraction, then combining this result with the appropriate water broadening coefficients in the retrieval of the other species.

Here we compare the effectiveness of these two approaches in the case of the QCLAS. Such comparison of these two methods is instructive to other experimentalists that may seek to apply similar corrections. Both approaches require empirical (laboratory) data, which can be obtained simultaneously for direct comparison.

As the empirical coefficients required by both methods can be determined using the same experiment, and given that TDLWintel retains the measured raw spectral data, it was possible to ~~do~~ perform this comparison by reanalysing the same dataset, either deriving a scale factor to post-process the data, or varying ~~only~~ the way in which the water vapour influence was treated in the retrieval. The data here was gathered in four separate laboratory experiments, each using an identical experimental setup to that employed by O'Shea et al. (2013b), who provide a full description. In summary, dry compressed air was humidified to a variety of different water vapour mole fractions, spanning the range of 0–2% typically measured in flight. Between each measurement of humid air, a dry reference was sampled, using a dry ice trap to reduce the sample dew point to less than – 60 °C. It should be noted that by re-drying the air downstream of the humidifier we accounted for any dissolution of gases in the humidifier, and the temperature dependence of this effect.

The first approach used the following relationship to scale the measurements of the wet sample to corresponding dry mole fractions:

$$X_{dry} = \frac{X_{wet}}{a + b H_2O} \quad (2)$$

where X_{wet} and X_{dry} are the raw and the scaled, water corrected mole fractions respectively for species X , and H_2O represents the retrieved mole fraction of water vapour. Coefficients a and b were derived by performing a weighted least orthogonal distance regression of X_{wet}/X_{dry} as a function of H_2O for data from all four experiments.

The empirical values for the QCLAS were found to be $a = 1.00096$, $b = -0.0154563 \text{ \%}^{-1}$ for N_2O , and $a = 1.00071$, $b = -0.0136929 \text{ \%}^{-1}$ for CH_4 . The uncertainties associated with these values can be quantified by the residuals of this regression for CH_4 and N_2O , shown in Fig. 2. The RMS (root mean square) values for these residuals are 2.5 ppb and 0.50 ppb for CH_4 and N_2O respectively.

It is apparent from Fig. 2 that substantially different behaviour was observed on 20 ~~June~~ ~~/06/20~~14 when compared to the three other experiments. This is likely to be associated with a lack of long-term stability in the retrieval of H_2O mole fraction, as indicated by the drift in the average retrieved H_2O mole fraction during the dry runs seen in Fig. 2. As this is a measurement of very dry air (less than $-60 \text{ }^\circ\text{C}$ dew point), this drift can be assumed to represent the variability in the baseline intensity in the region of the H_2O absorption line, likely resulting from very small changes in the optical alignment and/or pathlength. This subtle variability in baseline intensity then manifests as systematic variability in the accuracy of the retrieved H_2O mole fractions. The consequence of this on the long-term stability of the scale factor method, and the improvement gained using the spectroscopic correction, are discussed below. ~~largely driven by variability in baseline intensity in the region of the H_2O absorption line. The effect of this baseline instability can be reduced by using the spectroscopic water vapour correction method described below.~~

The second, spectroscopic, water vapour correction method used the water broadening function in TDLWintel to correct for the influence of water vapour. Reanalyses of the raw spectra were performed using a variety of different water broadening coefficients in the retrieval. For each coefficient, the difference between the retrieved wet mole fraction and the corresponding dry measurement was calculated at every water vapour level used during the four experiments. The RMS difference for each coefficient, averaged over the entire dataset, is shown in Fig. 3. It can be seen that the correction performed best using water broadening coefficients of 1.6 and 1.8 for CH_4 and N_2O respectively. These optimal coefficients resulted in RMS differences between corresponding wet and dry measurements of 1.6 ppb for CH_4 and 0.32 ppb for N_2O ; these are the values used to determine the contribution of uncertainty in this water vapour correction to the total measurement uncertainty of the instrument.

It was thus concluded that in this case a better correction for the influence of water vapour was obtained using the spectroscopic correction performed by the TDLWintel software than was achieved by scaling the wet mole fractions according to Eq. (2). There are two potential

factors that could explain the improved performance of the spectroscopic method over the scale factor method. Firstly, because the spectroscopic correction determines the water vapour pressure broadening relative to the dry air pressure broadening, it implicitly accounts for changes in absolute water vapour pressure associated with corresponding changes in measured sample cell pressure. In contrast, the scale factor method using Eq. (2) relies only on the retrieved mole fraction of water vapour, and so fails to account for any increase or decrease in water vapour pressure broadening at higher or lower cell pressures.

Secondly, in the scale factor method, drift in the uncalibrated water vapour mole fraction measurements propagates directly via Eq. (2) into a systematic error in the water corrected mole fraction for both CH_4 and N_2O (X_{dry}). In the spectroscopic method, inaccuracies in the measurement of water vapour mole fraction instead impact upon the subsequent retrieval of CH_4 and N_2O by affecting the fitting of the Voigt line profile. Although inaccurately calculated water vapour line broadening will change the retrieved mole fraction using the spectroscopic method, because the water vapour broadening is just one of several parameters constraining the spectral fit, inaccuracy resulting from this effect will be manifest in part as a reduction in the goodness of fit (spectral residual). Hence the spectroscopic method is less sensitive to any potential drift in the retrieval of water vapour mole fraction than the scale factor method.

All flight data presented in this paper has been reanalysed using this spectroscopic water vapour correction, with empirically derived water broadening coefficients of 1.6 and 1.8 for CH_4 and N_2O respectively.

3 Data Quality

Systematic instrumental error associated with changes in external variables such as temperature and pressure can be compensated for by repeated sampling of calibration gas. During airborne sampling an instrument is exposed to rapid changes in these variables over a wide range of values, hence regular calibration is required.

In this section we first describe the calibration procedure used during the two campaigns, and explain the rationale behind it. We then seek to diagnose and understand the sources of systematic error which remain uncaptured by this calibration. Finally, we describe an

alternative calibration procedure designed to better address these key sources of error, and evaluate the effect of both methods on the overall data quality.

3.1 Original Calibration Procedure

The in-flight calibration procedure employed throughout the GAUGE and MAMM campaigns was in principle similar to that described by O'Shea et al. (2013b). The data was scaled using two cylinders of known composition, traceable to the WMO greenhouse gas scale (WMO, 2009), whose mole fractions spanned the normal measurement range for N₂O and CH₄. By sequentially pumping gas from these cylinders through the system and comparing the retrieved mole fractions to their WMO-traceable values, two reference points could be established for the QCLAS on the WMO scale. By assuming a linear relationship, the "true" mole fraction corresponding to each retrieved QCLAS mole fraction was given by interpolating the scale between the two reference points. For each calibration a scale factor (M_x) and zero-offset (C_x) were found using:

$$M_x = \frac{(X_{high, WMO} - X_{low, WMO})}{(X_{high, meas} - X_{low, meas})} \quad (3)$$

$$C_x = X_{high, WMO} - M_x \cdot X_{high, meas} \quad (4)$$

where $X_{high, WMO}$ and $X_{low, WMO}$ are the "true" WMO-traceable mole fraction values, and $X_{high, meas}$ and $X_{low, meas}$ are the measured mole fraction values, for the high and low calibration cylinders respectively, for a given species X .

These two cylinders were sampled sequentially on an approximately hourly basis and the values for M_x and C_x were linearly interpolated between calibrations. The raw data was then calibrated by applying:

$$X_{cal}(t) = M_x(t) \cdot X_{raw}(t) + C_x(t) \quad (5)$$

In order to check that both interpolation between the two cylinder mole fraction values and temporal interpolation between hourly calibrations were justified, a third WMO-traceable "target" cylinder containing intermediate CH₄ and N₂O mole fractions was measured approximately mid-way between the hourly high-low span calibrations. Applying the above calibration to this target cylinder measurement and comparing the resulting calibrated mole fractions with the WMO-traceable values for the cylinder enabled errors associated with this

method to be quantified. Raw CH₄ data demonstrating a typical calibration cycle is shown in Fig. 4.

This calibration procedure was designed to remove linear drifts acting over timescales of the order of the inter-calibration time, here approximately 1 hour. However, analysis of the difference in CH₄ mole fraction between the raw QCLAS data and the calibrated data from the on-board FGGA frequently showed gradients of over 30 ppb in timescales of less than 10 minutes, as shown for flight B848 in Fig. 5. The FGGA on board the FAAM aircraft has previously been shown not to exhibit any significant systematic errors on this timescale (O'Shea et al., 2013b), suggesting that these gradients represent a source of systematic error in the QCLAS data. Note that although we have compensated here for the lag time between the two instruments using the correlation between the two CH₄ datasets, large deviations from the overall trend with very short durations are present as a result of small differences in the measurement time of large CH₄ enhancements.

Figure 6 shows the same CH₄ data from flight B848 plotted as a function of static pressure, as measured by the aircraft's RVSM (Reduced Vertical Separation Minimum) system. It can be seen that a broadly repeatable pattern exists as a function of pressure, which was found to dominate variability in the raw QCLAS CH₄ data offset with respect to the FGGA over the course of the flight. The same pattern is also exhibited by the offset of the calibration cylinder measurements from the nominal values of the cylinders (also shown), although the absolute value of this offset clearly differs between the cylinders. Similar patterns were observed for the cylinder measurements of N₂O, and across other flights during the two campaigns.

The fact that this variation with pressure can be observed in both the raw sample data and the measurement of dry calibration air confirms that errors in the water vapour correction cannot be responsible. A leak (ingress) into the system also appears implausible, as one would expect this to have the opposite effect on the high and low cylinder measurements, pulling both towards the mole fractions of CH₄ and N₂O present in the aircraft cabin. Santoni et al. (2014) warn of issues associated with fluctuations in sample cell pressure. However, the offsets in retrieved QCLAS mole fractions observed here were found to exhibit no dependence on either sample cell pressure or sample cell temperature, or the rate of change for these variables (as recorded by the pressure and temperature sensors within the sample flow).

The temperature of the cabin air was also recorded as it entered the outer enclosure of the QCLAS, but this again exhibited no clear correlation with the CH₄ data offset. The pressure

inside the cabin, however, was not recorded during ~~these~~ the 2014 campaigns. Subsequent test flights, described in Sect. 3.2 below, suggest that it was variability in this quantity that caused the large gradients in CH₄ offset described above.

3.2 Influence of Cabin Pressure

In April 2015 we performed a test flight, (B903), ~~was flown~~ designed to further understanding of the underlying issues behind the large gradients in QCLAS CH₄ data described in Sect. 3.1 above. This time cabin pressure data was available throughout the flight, and three deep profiles were performed whilst the QCLAS sampled compressed air from a calibration cylinder. The first deep profile occurred at the beginning of the flight, whilst the other two were performed ~ 2.5 hours later.

Figure 7 shows the offset in retrieved CH₄ and N₂O mole fractions from the known composition of the cylinder as a function of both cabin pressure and RVSM external static pressure. For external pressures between ~ 800 hPa and ~ 1000 hPa these offsets remain roughly constant; this can be seen to correspond to the range of external pressures over which there is no change in cabin pressure. The fact that, for both CH₄ and N₂O, the raw QCLAS measurement offset does not change when the cabin pressure is constant, even when the external pressure is varying, strongly suggests that cabin pressure variability is the primary cause of the large gradients in this offset observed throughout the GAUGE and MAMM campaigns in summer 2014.

A time series of the retrieved mole fraction offsets for the final two profiles is shown in Fig. 8. The influence of changing cabin pressure on these retrieved mole fractions can be characterised as a small scale oscillation superimposed on a larger scale gradient. This large scale gradient appears to be very consistent across the three profiles (see also Fig. 7), whereas the small scale oscillations are not so repeatable.

The likely pathway through which cabin pressure can influence the retrieved mole fractions is through its effect on baseline intensity in the spectral regions close to the absorption lines. There are two potential components to this: the effect of changing absorption in the open path section of the laser, and the effect of changing pressure on the alignment of , and spacing between, the instrument's optical components.

To investigate the effect of varying the open path absorption, a further test flight was conducted whilst flowing dry nitrogen through the laser beam enclosure. A simulation was

also performed, where open path CH₄ and N₂O absorption were included in the spectral fit for the range of cabin pressures encountered during flight B903, to assess the impact on the retrieved mole fractions. Both of these tests indicated that varying open path absorption contributed negligibly to the observed gradients in retrieved mole fraction over the range of cabin pressures experienced during these flights. Hence we conclude that these gradients are more likely attributable to small changes in optical alignment/[spacing](#) associated with cabin pressure variation.

3.3 Pressure-Differentiated Calibration Procedure

As the short term (of order minutes) instrumental drift with pressure had a greater effect in degrading measurement precision than any longer term (of order hours) drift with time, the data was reanalysed using an alternative calibration procedure, designed to reduce the impact of this issue on the overall accuracy of the calibrated measurements. As there was no cabin pressure data available for the GAUGE and MAMM campaigns in summer 2014, it was necessary to use the external static pressure from the aircraft's RVSM system as a proxy. This approach is justified by the strong correlation between cabin pressure and external pressure, and by the results in Sect. 3.4 below.

In this approach values of $M_x(t)$ and $C_x(t)$ for sections of flight at broadly equivalent pressure levels (defined here as a range of variability less than 15 hPa for a period longer than 2 minutes) were interpolated between any calibrations conducted at a pressure within 15 hPa of the average pressure during that section. Profile data, along with all data at pressure levels where no calibrations were performed, were flagged as poor quality and removed from the analysis. This pressure-differentiated calibration method has the disadvantages of both reducing the amount of calibrated data for the campaigns by 54% and potentially inducing errors associated with long term instrumental drift, as data can be separated from the corresponding calibration(s) by up to 5 hours. The effect on the overall data quality of using this pressure-differentiated calibration procedure is discussed and compared in Sect. 3.4.

It was also found that large roll angles (~ 20° or over), associated with sharp turns of the aircraft, produced short term deviations in retrieved CH₄ and N₂O mole fractions, evident in both the raw and calibrated data. It is likely that this effect is a consequence of slight alignment changes (similar to Sect 3.2 above) caused by the centrifugal force of the turn (no relationship with cabin pressure variability was found). Whilst this effect was clearly secondary to the pressure-dependent variability described above, producing CH₄ deviations of

less than 5 ppb, it was decided to flag all data associated with roll angles of greater than 10° as reduced quality. All calibrated data (using both methods) discussed here has been filtered according to this flag, removing the reduced quality data associated with high roll angles. The application of this filter reduces the total size of the raw dataset by only 7%.

3.4 Results and Discussion

The performance of the QCLAS can be assessed both by comparing the calibrated target cylinder measurements to their corresponding WMO-traceable values and by comparing the calibrated 1 Hz CH₄ sample data with the corresponding measurements from the on-board FGGA. No other instruments on board the FAAM aircraft measured N₂O during the GAUGE or MAMM campaigns, so a direct comparison of sample N₂O mole fractions cannot be made here. Table 1 summarises these results for both the original calibration method described in Sect. 3.1 and the pressure-differentiated calibration method described in Sect. 3.2.

It can be seen from the table that using the pressure-differentiated calibration method significantly improves the accuracy of the QCLAS, both during target cylinder measurements and sample mode. In particular, the standard deviations in QCLAS-target and QCLAS-FGGA differences are substantially reduced compared to the equivalent values produced using the original calibration method. The WMO recommends compatibility between different analyses within 2 ppb for CH₄ and 0.1 ppb for N₂O (WMO, 2013). The fraction of data within these ranges for both the QCLAS-target and QCLAS-FGGA differences using both methods is shown in Table 2. Here again it can be seen that the pressure-differentiated calibration method produces superior results.

Figure 9 shows the offset between the calibrated 1 Hz QCLAS target cylinder measurements and the known content of the cylinder, as histograms for both CH₄ and N₂O. It can be seen here that the improved standard deviations obtained using the pressure-differentiated calibration method result from the removal of outlying data associated with the pressure effect discussed in the previous section. Also shown are histograms of the QCLAS-FGGA offset for 1 Hz CH₄ sample data, which provide further evidence of the superior performance of the pressure-differentiated calibration method. The data produced using the original calibration method is clearly far less well represented by a Gaussian fit; this is to be expected in the presence of a systematic effect such as that described in Sect. 3 above. In contrast, the Gaussian shape of the pressure-differentiated data is consistent with a random error distribution for both instruments.

The instrument precision can be quantified using the Allan Variance technique (Werle et al., 1993). Table 3 presents the 1σ Allan Precision (over 1 s, 10 s and 108 s) for CH₄ and N₂O, both in a laboratory environment whilst sampling a compressed air cylinder, and in flight during a period of ambient background sampling. These results are similar to those of Santoni et al. (2014), with in-flight 1 Hz precisions here of 0.52 ppb for CH₄ and 0.11 ppb for N₂O.

Finally, a nominal uncertainty for the data can be calculated using the known uncertainties from the water vapour correction experiment, the calibration of the target cylinder to the WMO scale and the in-flight target measurements. Table 4 contains these values for both CH₄ and N₂O using the pressure-differentiated calibration method. The nominal total uncertainties for CH₄ and N₂O are $\pm 2.47 \pm 0.81$ ppb and $\pm 0.54 \pm 0.35$ ppb respectively.

4. Case Study

The GAUGE project aims to provide top-down greenhouse gas emission estimates for the UK, which can be used to validate the bottom-up inventory-based estimates required by UK and international legislation. As part of this approach, it is planned to use aircraft data in combination with mass balance techniques (Karion et al., 2013; O'Shea et al., 2014a; Peischl et al., 2015) to estimate regional greenhouse gas emissions. Such analysis is beyond the scope of this technical study, however we present QCLAS data from a single flight here as an exemplar of typical flight data, providing context with regard to scientific case studies which may use this new airborne dataset.

Flight B868 was designed to incorporate upwind and downwind sampling over northwest England to provide a dataset for a mass balance case study. This region contains several large urban areas (Manchester, Liverpool, Leeds and Sheffield) and also includes several areas of agricultural activity, known to be an important anthropogenic source of N₂O (Syakila and Kroeze, 2011). The flight track, coloured by N₂O mole fraction, is shown in Fig. 10. The wind speed and direction, as measured on board the aircraft and taken as an average over 60 s, are represented by wind barbs, according to the standard convention where each full barb represents a wind speed of 10 knots. Selected Lagrangian back trajectories using the HYSPLIT (Hybrid Single-Particle Lagrangian Integrated Trajectory) model (Draxler and Hess, 1998) are also shown (representing around 24 hours track across the UK mainland in the figure). These trajectories were initiated using endpoints and trajectory end-times selected

1 along the flight track, and modelled with full vertical dynamics using Global Data
2 Assimilation System 1° resolution data.

3 It can be seen that the N₂O mole fractions measured in the northwest of the domain were
4 enhanced relative to those in the southeast. A relatively consistent south-easterly wind
5 direction (both measured and seen in the trajectories) suggests that this enhancement may
6 enable the use of a mass balance technique to estimate the N₂O flux from an area between this
7 downwind transect and the corresponding upwind measurements using the techniques
8 described by O'Shea et al. (2014a). This requires suitable investigation of the necessary
9 assumptions, which is beyond the scope of this simple example.

10 It is also striking that there is a relative contrast in the southwest area of the domain, with N₂O
11 mole fractions around 328 ppb (compared with 330 ppb in the northwest). The potential
12 reasons for this small contrast, in terms of air mass history, may be explained by considering
13 both the trajectories and the wind barbs. The trajectories from the northwest domain show
14 recent transport at low altitude (below 1 km) over Greater Manchester and the North West
15 conurbation, whereas southwest trajectories pass over more rural areas. This appears
16 counterintuitive, as we expect the agricultural sector to be the primary contributor towards
17 N₂O emissions in this region. However, the wind barbs (which represent real measurements)
18 show that there is a complex divergence in the wind-field in the southwest domain, perhaps
19 indicative of a localised sea-breeze circulation that cannot be expected to have been captured
20 at the resolution of the meteorological data that was used to initialise the HYSPLIT
21 trajectories. This sea-breeze circulation could suggest recirculation of maritime air and hence
22 dilution of any moderately enhanced air arriving on the prevailing wind from the east. The
23 differing localised dynamics and air mass histories of the two domains may explain the
24 observed contrast. Further analysis of this may form the basis of future work and this limited
25 example demonstrates the utility of aircraft data in understanding local and regional air mass
26 characteristics.

27 28 **5. Conclusions**

29 ~~An Aerodyne Research Inc. QCLAS~~ A Quantum Cascade Laser Absorption Spectrometer was
30 used to measure N₂O and CH₄ on board the FAAM aircraft during the GAUGE and MAMM
31 campaigns in summer 2014. A relationship between QCLAS measurement error and cabin
32 pressure was found, and a new calibration procedure was adopted to minimise the impact of

1 this effect on the final data. Using this pressure-differentiated calibration method, total
2 uncertainties of $\pm \text{2.474-81}$ ppb and $\pm \text{0.540-35}$ ppb were obtained for the measurement of
3 CH₄ and N₂O respectively.

4 The sample air was not dried prior to measurement, so a correction for the influence of water
5 vapour on the retrieved mole fractions was required. The performance of two different water
6 vapour correction methods was compared using data from four separate experiments. It was
7 found that the best results were obtained using the water broadening function in the
8 TDLWintel software, which included the effects of water broadening on the CH₄ and N₂O
9 absorption lines directly in the mole fraction retrieval. Experimentally derived coefficients for
10 the ratio of water vapour broadening to air broadening of 1.6 and 1.8 were found to give the
11 best results for CH₄ and N₂O respectively.

12 Overall instrument performance is found to be broadly comparable with similar studies (e.g.
13 O'Shea et al., 2013b; Santoni et al., 2014) if the pressure-differentiated calibration procedure
14 is used. However, this has the disadvantage of removing 54% of the measured sample data,
15 including all data during vertical profiles, which are frequently of scientific interest. A
16 priority for improvement is to prevent the large short term drifts in measurement error that
17 necessitate the removal of this data. One potential solution would be to enclose the instrument
18 within a pressure-sealed container. The feasibility of practically implementing this solution on
19 board the FAAM aircraft is currently being studied.

20 **Acknowledgements**

21 The authors would like to thank everyone at FAAM and the numerous people at Avalon Aero
22 and Directflight who assisted with the logistics of installing the QCLAS on the aircraft. J.R.
23 Pitt is in receipt of a NERC CASE studentship in partnership with FAAM, grant number
24 NE/L501/591/1, supervised by G. Allen. This work was supported by the NERC projects:
25 GAUGE (Greenhouse gAs UK and Global Emissions), grant number NE/K002279/1, and
26 MAMM (Methane and other greenhouse gases in the Arctic: Measurements, process studies
27 and Modelling), grant number NE/I029161/1. We are also grateful to the Norwegian Research
28 Council, who partly funded the 2014 MAMM flights through the MOCA (Methane Emissions
29 from the Arctic Ocean to the Atmosphere: Present and Future Climate Effects) project.

1 **References**

- 2 Allen, G., Illingworth, S. M., O'Shea, S. J., Newman, S., Vance, A., Bauguitte, S. J.-B.,
3 Marengo, F., Kent, J., Bower, K., Gallagher, M. W., Muller, J., Percival, C. J., Harlow, C.,
4 Lee, J. and Taylor, J. P.: Atmospheric composition and thermodynamic retrievals from the
5 ARIES airborne TIR-FTS system – Part 2: Validation and results from aircraft campaigns,
6 *Atmos. Meas. Tech.*, 7, 4401–4416, doi:10.5194/amt-7-4401-2014, 2014.
- 7 Baer, D. S., Paul, J. B., Gupta, M. and O'Keefe, A.: Sensitive absorption measurements in the
8 near-infrared region using off-axis integrated-cavity-output spectroscopy, *Appl. Phys. B-*
9 *Lasers O.*, 75, 261–265, doi:10.1007/s00340-002-0971-z, 2002.
- 10 Chen, H., Winderlich, J., Gerbig, C., Hofer, A., Rella, C. W., Crosson, E. R., Van Pelt, A.
11 D., Steinbach, J., Kolle, O., Beck, V., Daube, B. C., Gottlieb, E. W., Chow, V. Y., Santoni, G.
12 W. and Wofsy, S. C.: High-accuracy continuous airborne measurements of greenhouse gases
13 (CO₂ and CH₄) using the cavity ring-down spectroscopy (CRDS) technique, *Atmos. Meas.*
14 *Tech.*, 3, 375–386, doi:10.5194/amt-3-375-2010, 2010.
- 15 Ciais, P., Sabine, C., Bala, G., Bopp, L., Brovkin, V., Canadell, J., Chhabra, A., DeFries, R.,
16 Galloway, J., Heimann, M., Jones, C., Quéré, C. Le, Myneni, R. B., Piao, S. and Thornton, P.:
17 Carbon and Other Biogeochemical Cycles, in: *Climate Change 2013: The Physical Science*
18 *Basis. Contribution of Working Group I to the Fifth Assessment Report of the*
19 *Intergovernmental Panel on Climate Change*, edited by T. F. Stocker, D. Qin, G.-K. Plattner,
20 M. Tignor, S. K. Allen, J. Boschung, A. Nauels, Y. Xia, V. Bex, and P. M. Midgley,
21 Cambridge University Press, Cambridge, United Kingdom and New York, NY, USA, 465–
22 570, 2013.
- 23 Crosson, E. R.: A cavity ring-down analyzer for measuring atmospheric levels of methane,
24 carbon dioxide, and water vapor, *Appl. Phys. B-Lasers O.*, 92, 403–408, doi:10.1007/s00340-
25 008-3135-y, 2008.
- 26 Daube, B. C., Boering, K. A., Andrews, A. E. and Wofsy, S. C.: A High-Precision Fast-
27 Response Airborne CO₂ Analyzer for In Situ Sampling from the Surface to the Middle
28 Stratosphere, *J. Atmos. Ocean. Tech.*, 19, 1532–1543, doi:10.1175/1520-
29 0426(2002)019<1532:AHPFRA>2.0.CO;2, 2002.
- 30 Draxler, R. R. and Hess, G. D.: An Overview of the HYSPLIT_4 Modelling System for
31 Trajectories, Dispersion, and Deposition., *Aust. Meteorol. Mag.*, 47, 295–308, 1998.
- 32 Ebi, K. L. and McGregor, G.: Climate change, tropospheric ozone and particulate matter, and
33 health impacts., *Environ. Health Persp.*, 116, 1449–1455, doi:10.1289/ehp.11463, 2008.
- 34 Fraser, A., Palmer, P. I., Feng, L., Boesch, H., Cogan, A., Parker, R., Dlugokencky, E. J.,
35 Fraser, P. J., Krummel, P. B., Langenfelds, R. L., O'Doherty, S., Prinn, R. G., Steele, L. P.,
36 van der Schoot, M. and Weiss, R. F.: Estimating regional methane surface fluxes: the relative
37 importance of surface and GOSAT mole fraction measurements, *Atmos. Chem. Phys.*, 13,
38 5697–5713, doi:10.5194/acp-13-5697-2013, 2013.

- 1 Hartmann, D. J., Klein Tank, A. M. G., Rusticucci, M., Alexander, L. V., Brönnimann, S.,
2 Charabi, Y. A.-R., Dentener, F. J., Dlugokencky, E. J., Easterling, D. R., Kaplan, A., Soden,
3 B. J., Thorne, P. W., Wild, M. and Zhai, P.: Observations: Atmosphere and Surface, in:
4 Climate Change 2013: The Physical Science Basis. Contribution of Working Group I to the
5 Fifth Assessment Report of the Intergovernmental Panel on Climate Change, edited by T. F.
6 Stocker, D. Qin, G.-K. Plattner, M. Tignor, S. K. Allen, J. Boschung, A. Nauels, Y. Xia, V.
7 Bex, and P. M. Midgley, Cambridge University Press, Cambridge, United Kingdom and New
8 York, NY, USA, 159–254, 2013.
- 9 Hiller, R. V, Neininger, B., Brunner, D., Gerbig, C., Bretscher, D., Künzle, T., Buchmann, N.
10 and Eugster, W.: Aircraft-based CH₄ flux estimates for validation of emissions from an
11 agriculturally dominated area in Switzerland, *J. Geophys. Res.-Atmos.*, 119, 4874–4887,
12 doi:10.1002/2013JD020918.Received, 2014.
- 13 Karion, A., Sweeney, C., Pétron, G., Frost, G., Michael Hardesty, R., Kofler, J., Miller, B. R.,
14 Newberger, T., Wolter, S., Banta, R., Brewer, A., Dlugokencky, E., Lang, P., Montzka, S. A.,
15 Schnell, R., Tans, P., Trainer, M., Zamora, R. and Conley, S.: Methane emissions estimate
16 from airborne measurements over a western United States natural gas field, *Geophys. Res.*
17 *Lett.*, 40, 4393–4397, doi:10.1002/grl.50811, 2013.
- 18 Kirschke, S., Bousquet, P., Ciais, P., Saunio, M., Canadell, J. G., Dlugokencky, E. J.,
19 Bergamaschi, P., Bergmann, D., Blake, D. R., Bruhwiler, L., Cameron-Smith, P., Castaldi, S.,
20 Chevallier, F., Feng, L., Fraser, A., Heimann, M., Hodson, E. L., Houweling, S., Josse, B.,
21 Fraser, P. J., Krummel, P. B., Lamarque, J.-F., Langenfelds, R. L., Le Quéré, C., Naik, V.,
22 O'Doherty, S., Palmer, P. I., Pison, I., Plummer, D., Poulter, B., Prinn, R. G., Rigby, M.,
23 Ringeval, B., Santini, M., Schmidt, M., Shindell, D. T., Simpson, I. J., Spahni, R., Steele, L.
24 P., Strode, S. A., Sudo, K., Szopa, S., van der Werf, G. R., Voulgarakis, A., van Weele, M.,
25 Weiss, R. F., Williams, J. E. and Zeng, G.: Three decades of global methane sources and
26 sinks, *Nat. Geosci.*, 6, 813–823, doi:10.1038/ngeo1955, 2013.
- 27 Kort, E. A., Eluszkiewicz, J., Stephens, B. B., Miller, J. B., Gerbig, C., Nehrkorn, T., Daube,
28 B. C., Kaplan, J. O., Houweling, S. and Wofsy, S. C.: Emissions of CH₄ and N₂O over the
29 United States and Canada based on a receptor-oriented modeling framework and COBRA-NA
30 atmospheric observations, *Geophys. Res. Lett.*, 35, 1–5, doi:10.1029/2008GL034031, 2008.
- 31 Kort, E. A., Wofsy, S. C., Daube, B. C., Diao, M., Elkins, J. W., Gao, R. S., Hints, E. J.,
32 Hurst, D. F., Jimenez, R., Moore, F. L., Spackman, J. R. and Zondlo, M. A.: Atmospheric
33 observations of Arctic Ocean methane emissions up to 82° north, *Nat. Geosci.*, 5, 318–321,
34 doi:10.1038/ngeo1452, 2012.
- 35 Krinner, G., Viovy, N., de Noblet-Ducoudré, N., Ogée, J., Polcher, J., Friedlingstein, P.,
36 Ciais, P., Sitch, S. and Prentice, I. C.: A dynamic global vegetation model for studies of the
37 coupled atmosphere-biosphere system, *Global Biogeochem. Cy.*, 19, 1–33,
38 doi:10.1029/2003GB002199, 2005.
- 39 McManus, J. B., Keabian, P. L. and Zahniser, M. S.: Astigmatic mirror multipass absorption
40 cells for long-path-length spectroscopy, *Appl. Optics*, 34, 3336–3348,
41 doi:10.1364/AO.34.003336, 1995.

- 1 Miller, S. M., Wofsy, S. C., Michalak, A. M., Kort, E. A., Andrews, A. E., Biraud, S. C.,
2 Dlugokencky, E. J., Eluszkiewicz, J., Fischer, M. L., Janssens-Maenhout, G., Miller, B. R.,
3 Miller, J. B., Montzka, S. A., Nehrkorn, T. and Sweeney, C.: Anthropogenic emissions of
4 methane in the United States., *P. Natl. Acad. Sci. USA*, 110, 20018–20022,
5 doi:10.1073/pnas.1314392110, 2013.
- 6 Myhre, G., Shindell, D., Bréon, F.-M., Collins, W., Fuglestad, J., Huang, J., Koch, D.,
7 Lamarque, J.-F., Lee, D., Mendoza, B., Nakajima, T., Robock, A., Stephens, G., Takemura, T.
8 and Zhang, H.: Anthropogenic and Natural Radiative Forcing, in: *Climate Change 2013: The*
9 *Physical Science Basis. Contribution of Working Group I to the Fifth Assessment Report of*
10 *the Intergovernmental Panel on Climate Change*, edited by T. F. Stocker, D. Qin, G.-K.
11 Plattner, M. Tignor, S. K. Allen, J. Boschung, A. Nauels, Y. Xia, V. Bex, and P. M. Midgley,
12 Cambridge University Press, Cambridge, United Kingdom and New York, NY, USA, 659–
13 740, 2013.
- 14 Nelson, D. D., Shorter, J. H., McManus, J. B. and Zahniser, M. S.: Sub-part-per-billion
15 detection of nitric oxide in air using a thermoelectrically cooled mid-infrared quantum
16 cascade laser spectrometer, *Appl. Phys. B-Lasers O.*, 75, 343–350, doi:10.1007/s00340-002-
17 0979-4, 2002.
- 18 Nelson, D. D., McManus, B., Urbanski, S., Herndon, S. and Zahniser, M. S.: High precision
19 measurements of atmospheric nitrous oxide and methane using thermoelectrically cooled mid-
20 infrared quantum cascade lasers and detectors., *Spectrochim. Acta. A.*, 60, 3325–3335,
21 doi:10.1016/j.saa.2004.01.033, 2004.
- 22 O’Shea, S. J., Allen, G., Gallagher, M. W., Bauguitte, S. J.-B., Illingworth, S. M., Le Breton,
23 M., Muller, J. B. A., Percival, C. J., Archibald, A. T., Oram, D. E., Parrington, M., Palmer, P.
24 I. and Lewis, A. C.: Airborne observations of trace gases over boreal Canada during
25 BORTAS: campaign climatology, air mass analysis and enhancement ratios, *Atmos. Chem.*
26 *Phys.*, 13, 12451–12467, doi:10.5194/acp-13-12451-2013, 2013a.
- 27 O’Shea, S. J., Bauguitte, S. J.-B., Gallagher, M. W., Lowry, D. and Percival, C. J.:
28 Development of a cavity-enhanced absorption spectrometer for airborne measurements of
29 CH₄ and CO₂, *Atmos. Meas. Tech.*, 6, 1095–1109, doi:10.5194/amt-6-1095-2013, 2013b.
- 30 O’Shea, S. J., Allen, G., Fleming, Z. L., Bauguitte, S. J.-B., Percival, C. J., Gallagher, M. W.,
31 Lee, J., Helfter, C. and Nemitz, E.: Area fluxes of carbon dioxide, methane, and carbon
32 monoxide derived from airborne measurements around Greater London: A case study during
33 summer 2012, *J. Geophys. Res.-Atmos.*, 119, 4940–4952, doi:10.1002/2013JD021269,
34 2014a.
- 35 O’Shea, S. J., Allen, G., Gallagher, M. W., Bower, K., Illingworth, S. M., Muller, J. B. A.,
36 Jones, B., Percival, C. J., Bauguitte, S. J.-B., Cain, M., Warwick, N., Quicket, A., Skiba, U.,
37 Drewer, J., Dinsmore, K., Nisbet, E. G., Lowry, D., Fisher, R. E., France, J. L., Aurela, M.,
38 Lohila, A., Hayman, G., George, C., Clark, D., Manning, A. J., Friend, A. D. and Pyle, J.:
39 Methane and carbon dioxide fluxes and their regional scalability for the European Arctic
40 wetlands during the MAMM project in summer 2012, *Atmos. Chem. Phys.*, 14, 13159–
41 13174, 2014b.

1 Peischl, J., Ryerson, T. B., Holloway, J. S., Parrish, D. D., Trainer, M., Frost, G. J., Aikin, K.
2 C., Brown, S. S., Dubé, W. P., Stark, H. and Fehsenfeld, F. C.: A top-down analysis of
3 emissions from selected Texas power plants during TexAQS 2000 and 2006, *J. Geophys.*
4 *Res.*, 115, D16303, doi:10.1029/2009JD013527, 2010.

5 Peischl, J., Ryerson, T. B., Aikin, K. C., Gouw, J. A., Gilman, J. B., Holloway, J. S., Lerner,
6 B. M., Nadkarni, R., Neuman, J. A., Nowak, J. B., Trainer, M., Warneke, C. and Parrish, D.
7 D.: Quantifying atmospheric methane emissions from the Haynesville, Fayetteville, and
8 northeastern Marcellus shale gas production regions, *J. Geophys. Res.-Atmos.*, 120, 2119–
9 2139, doi:10.1002/2014JD022697, 2015.

10 Polson, D., Fowler, D., Nemitz, E., Skiba, U., McDonald, A., Famulari, D., Di Marco, C.,
11 Simmons, I., Weston, K. and Purvis, R.: Estimation of spatial apportionment of greenhouse
12 gas emissions for the UK using boundary layer measurements and inverse modelling
13 technique, *Atmos. Environ.*, 45, 1042–1049, doi:10.1016/j.atmosenv.2010.10.011, 2011.

14 Rannik, Ü., Haapanala, S., Shurpali, N. J., Mammarella, I., Lind, S., Hyvönen, N., Peltola, O.,
15 Zahniser, M., Martikainen, P. J. and Vesala, T.: Intercomparison of fast response commercial
16 gas analysers for nitrous oxide flux measurements under field conditions, *Biogeosciences*, 12,
17 415–432, doi:10.5194/bg-12-415-2015, 2015.

18 Ravishankara, A. R., Daniel, J. S. and Portmann, R. W.: Nitrous Oxide (N₂O): The Dominant
19 Ozone-Depleting Substance Emitted in the 21st Century, *Science*, 123, 123–125,
20 doi:10.1126/science.1176985, 2007.

21 Rella, C. W., Chen, H., Andrews, A. E., Filges, A., Gerbig, C., Hatakka, J., Karion, A., Miles,
22 N. L., Richardson, S. J., Steinbacher, M., Sweeney, C., Wastine, B. and Zellweger, C.: High
23 accuracy measurements of dry mole fractions of carbon dioxide and methane in humid air,
24 *Atmos. Meas. Tech.*, 6, 837–860, doi:10.5194/amt-6-837-2013, 2013.

25 Ritter, J. A., Barrick, J. D. W., Sachse, G. W., Gregory, G. L., Woerner, M. A., Watson, C. E.,
26 Hill, G. F. and Collins, J. E.: Airborne flux measurements of trace species in an Arctic
27 boundary layer, *J. Geophys. Res.*, 97, 16601–16625, doi:10.1029/92JD01812, 1992.

28 Rothman, L. S., Gordon, I. E., Babikov, Y., Barbe, A., Chris Benner, D., Bernath, P. F., Birk,
29 M., Bizzocchi, L., Boudon, V., Brown, L. R., Campargue, A., Chance, K., Cohen, E. A.,
30 Coudert, L. H., Devi, V. M., Drouin, B. J., Fayt, A., Flaud, J.-M., Gamache, R. R., Harrison,
31 J. J., Hartmann, J.-M., Hill, C., Hodges, J. T., Jacquemart, D., Jolly, A., Lamouroux, J., Le
32 Roy, R. J., Li, G., Long, D. A., Lyulin, O. M., Mackie, C. J., Massie, S. T., Mikhailenko, S.,
33 Müller, H. S. P., Naumenko, O. V., Nikitin, A. V., Orphal, J., Perevalov, V., Perrin, A.,
34 Polovtseva, E. R., Richard, C., Smith, M. A. H., Starikova, E., Sung, K., Tashkun, S.,
35 Tennyson, J., Toon, G. C., Tyuterev, V. G. and Wagner, G.: The HITRAN2012 molecular
36 spectroscopic database, *J. Quant. Spectrosc. Ra.*, 130, 4–50, doi:10.1016/j.jqsrt.2013.07.002,
37 2013.

38 Santoni, G. W., Daube, B. C., Kort, E. A., Jiménez, R., Park, S., Pittman, J. V., Gottlieb, E.,
39 Xiang, B., Zahniser, M. S., Nelson, D. D., McManus, J. B., Peischl, J., Ryerson, T. B.,
40 Holloway, J. S., Andrews, A. E., Sweeney, C., Hall, B., Hints, E. J., Moore, F. L., Elkins, J.
41 W., Hurst, D. F., Stephens, B. B., Bent, J. and Wofsy, S. C.: Evaluation of the airborne

1 quantum cascade laser spectrometer (QCLS) measurements of the carbon and greenhouse gas
2 suite – CO₂, CH₄, N₂O, and CO – during the CalNex and HIPPO campaigns, *Atmos. Meas.*
3 *Tech.*, 7, 1509–1526, doi:10.5194/amt-7-1509-2014, 2014.

4 Syakila, A. and Kroeze, C.: The global nitrous oxide budget revisited, *Greenhouse Gas*
5 *Measurement and Management*, 1, 17–26, doi:10.3763/ghgmm.2010.0007, 2011.

6 Tanaka, T., Miyamoto, Y., Morino, I., MacHida, T., Nagahama, T., Sawa, Y., Matsueda, H.,
7 Wunch, D., Kawakami, S. and Uchino, O.: Aircraft measurements of carbon dioxide and
8 methane for the calibration of ground-based high-resolution Fourier Transform Spectrometers
9 and a comparison to GOSAT data measured over Tsukuba and Moshiri, *Atmos. Meas. Tech.*,
10 5, 2003–2012, doi:10.5194/amt-5-2003-2012, 2012.

11 Thompson, R. L., Ishijima, K., Saikawa, E., Corazza, M., Karstens, U., Patra, P. K.,
12 Bergamaschi, P., Chevallier, F., Dlugokencky, E., Prinn, R. G., Weiss, R. F., O'Doherty, S.,
13 Fraser, P. J., Steele, L. P., Krummel, P. B., Vermeulen, A., Tohjima, Y., Jordan, A., Haszpra,
14 L., Steinbacher, M., Van Der Laan, S., Aalto, T., Meinhardt, F., Popa, M. E., Moncrieff, J.
15 and Bousquet, P.: TransCom N₂O model inter-comparison - Part 2: Atmospheric inversion
16 estimates of N₂O emissions, *Atmos. Chem. Phys.*, 14, 6177–6194, doi:10.5194/acp-14-6177-
17 2014, 2014.

18 Webb, N., Broomfield, M., Brown, P., Buys, G., Cardenas, L., Murrells, T., Pang, Y., Passant,
19 N., Thistlethwaite, G. and Watterson, J.: UK Greenhouse Gas Inventory 1990 to 2012:
20 Annual Report for submission under the Framework Convention on Climate Change,
21 Department of Energy and Climate Change, Harwell, Didcot, Oxfordshire., 2014.

22 Wecht, K. J., Jacob, D. J., Wofsy, S. C., Kort, E. A., Worden, J. R., Kulawik, S. S., Henze, D.
23 K., Kopacz, M. and Payne, V. H.: Validation of TES methane with HIPPO aircraft
24 observations: Implications for inverse modeling of methane sources, *Atmos. Chem. Phys.*, 12,
25 1823–1832, doi:10.5194/acp-12-1823-2012, 2012.

26 Werle, P., Mücke, R. and Slemr, F.: The limits of signal averaging in atmospheric trace-gas
27 monitoring by tunable diode-laser absorption spectroscopy (TDLAS), *Appl. Phys. B-Photo.*,
28 57, 131–139, doi:10.1007/BF00425997, 1993.

29 WMO: GAW Report No. 185 Guidelines for the Measurement of Methane and Nitrous Oxide
30 and their Quality Assurance, 2009.

31 WMO: GAW Report No. 213, 17th WMO/IAEA Meeting on Carbon Dioxide, Other
32 Greenhouse Gases and Related Tracers Measurement Techniques (GGMT-2013), 2013.

33 Wofsy, S. C., the HIPPO Science Team and Cooperating Modellers and Satellite Teams:
34 HIAPER Pole-to-Pole Observations (HIPPO): fine-grained, global-scale measurements of
35 climatically important atmospheric gases and aerosols., *Philos. T. R. Soc. A*, 369, 2073–2086,
36 doi:10.1098/rsta.2010.0313, 2011.

37 Xiang, B., Miller, S. M., Kort, E. A., Santoni, G. W., Daube, B. C., Commane, R., Angevine,
38 W. M., Ryerson, T. B., Trainer, M. K., Andrews, A. E., Nehrkorn, T., Tian, H. and Wofsy, S.

- 1 C.: Nitrous oxide (N₂O) emissions from California based on 2010 CalNex airborne
2 measurements, *J. Geophys. Res.-Atmos.*, 118, 2809–2820, doi:10.1002/jgrd.50189, 2013.
- 3 Yuan, B., Kaser, L., Karl, T., Graus, M., Peischl, J., Campos, T. L., Shertz, S., Apel, E. C.,
4 Hornbrook, R. S., Hills, A., Gilman, J. B., Lerner, B. M., Warneke, C., Flocke, F. M.,
5 Ryerson, T. B., Guenther, A. B. and de Gouw, J. A.: Airborne flux measurements of methane
6 and volatile organic compounds (VOCs) over the Haynesville and Marcellus shale gas
7 production regions, *J. Geophys. Res.-Atmos.*, 120, doi:10.1002/2015JD023242, 2015.
- 8 Zahniser, M. S., Nelson, D. D., McManus, J. B., Keabian, P. L. and Lloyd, D.: Measurement
9 of trace gas fluxes using tunable diode laser spectroscopy, *Philosophical Transactions:*
10 *Physical Sciences and Engineering*, 351, 371–382, 1995.
- 11 Zellweger, C., Steinbacher, M. and Buchmann, B.: Evaluation of new laser spectrometer
12 techniques for in-situ carbon monoxide measurements, *Atmos. Meas. Tech.*, 5, 2555–2567,
13 doi:10.5194/amt-5-2555-2012, 2012.
- 14 Zhuang, Q., Melillo, J. M., Sarofim, M. C., Kicklighter, D. W., McGuire, A. D., Felzer, B. S.,
15 Sokolov, A., Prinn, R. G., Steudler, P. A. and Hu, S.: CO₂ and CH₄ exchanges between land
16 ecosystems and the atmosphere in northern high latitudes over the 21st century, *Geophys.*
17 *Res. Lett.*, 33, 2–6, doi:10.1029/2006GL026972, 2006.

18

Calibration Method	QCLAS-target difference (ppb)				QCLAS-FGGA difference (ppb)	
	N ₂ O		CH ₄		CH ₄	
	Mean	1 σ	Mean	1 σ	Mean	1 σ
Original	0.00319	0.960	0.253	4.78	-2.87	8.27
Pressure-differentiated	0.105	0.419	0.0668	1.71	-2.05	5.85

Table 1: Mean and standard deviation of the difference between QCLAS 1 Hz target cylinder measurements and the nominal cylinder values, and the difference between the 1 Hz QCLAS and the corresponding 1 Hz FGGA sample CH₄ measurements, using both the original and pressure-differentiated calibration methods.

Calibration Method	QCLAS-target		QCLAS-FGGA
	N ₂ O	CH ₄	CH ₄
Original	0.149	0.519	0.292
Pressure-differentiated	0.309	0.765	0.361

- 1 **Table 2:** The fraction of 1 Hz data within the WMO compatibility recommendations for
- 2 QCLAS target cylinder measurement and QCLAS/FGGA sample measurement, using both
- 3 the original and pressure-differentiated calibration methods.

	1σ Allan Precision (ppb)					
	1 s		10 s		108 s	
	Flight	Lab	Flight	Lab	Flight	Lab
CH ₄	0.52	0.48	0.31	0.17	0.23	0.12
N ₂ O	0.11	0.12	0.074	0.044	0.042	0.029

- 1 **Table 3:** Allan Precision for QCLAS measurement of CH₄ and N₂O, both during ambient in-
- 2 flight sampling and whilst sampling a compressed air cylinder in the laboratory, given for
- 3 averaging times of 1 s, 10 s and 108 s.

	1σ Uncertainty (ppb)			
	Water vapour correction	Target standard calibration	In-flight target measurements	Total
CH ₄	1.63	0.77	1.71 0.07	2.47 1.81
N ₂ O	0.32	0.11	0.42 0.10	0.54 0.35

- 1 **Table 4:** Known component and nominal total uncertainties for the QCLAS measurement of
- 2 CH₄ and N₂O, calibrated using the pressure-differentiated method.

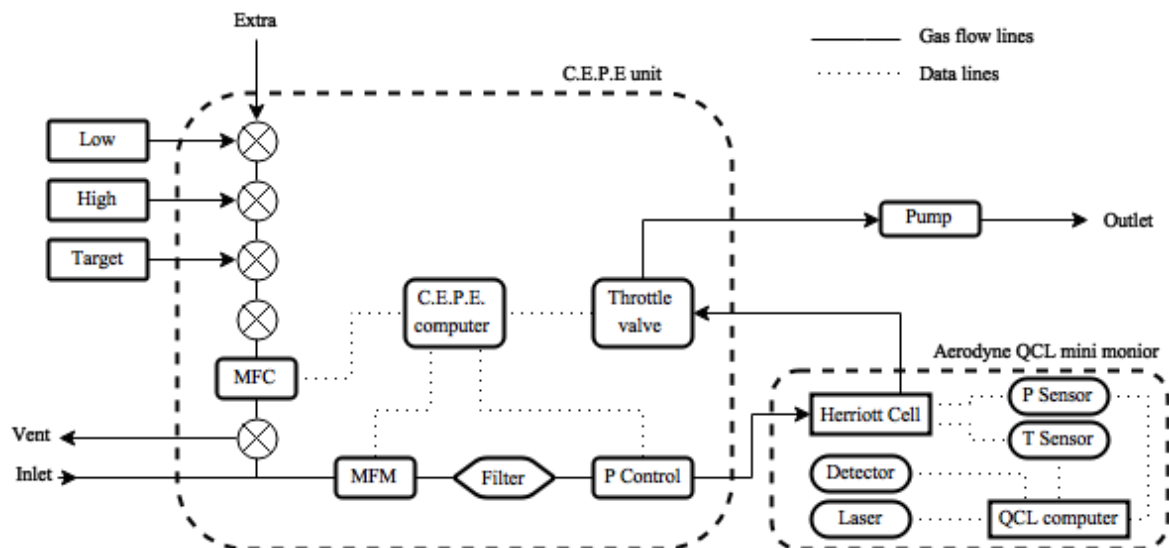
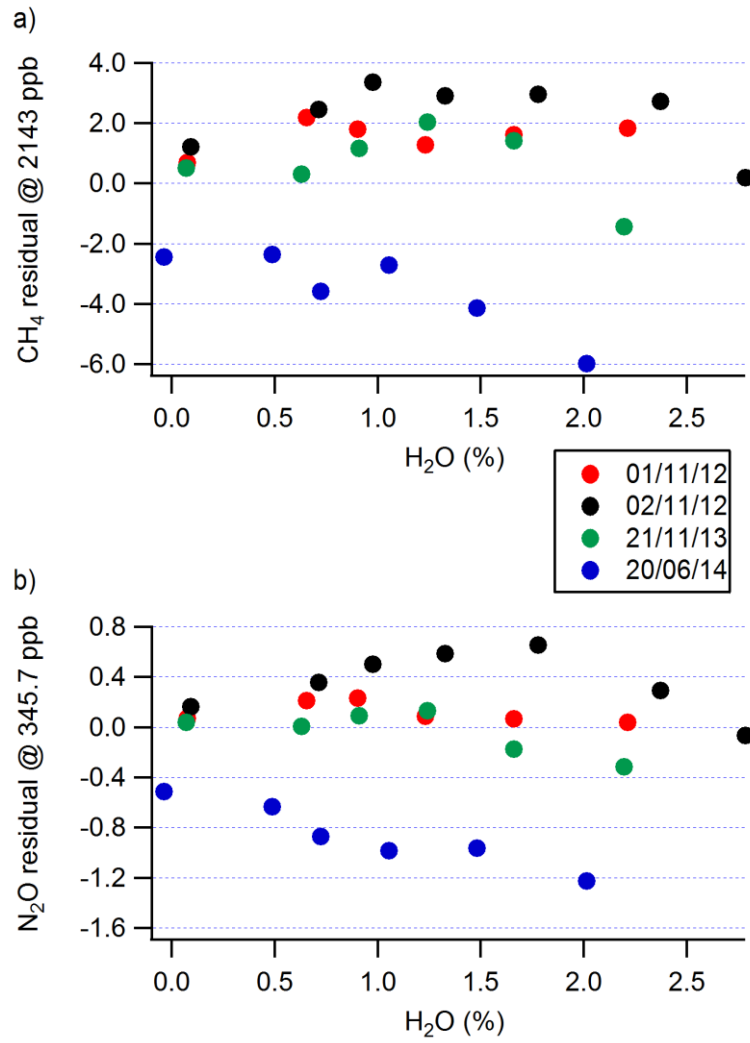
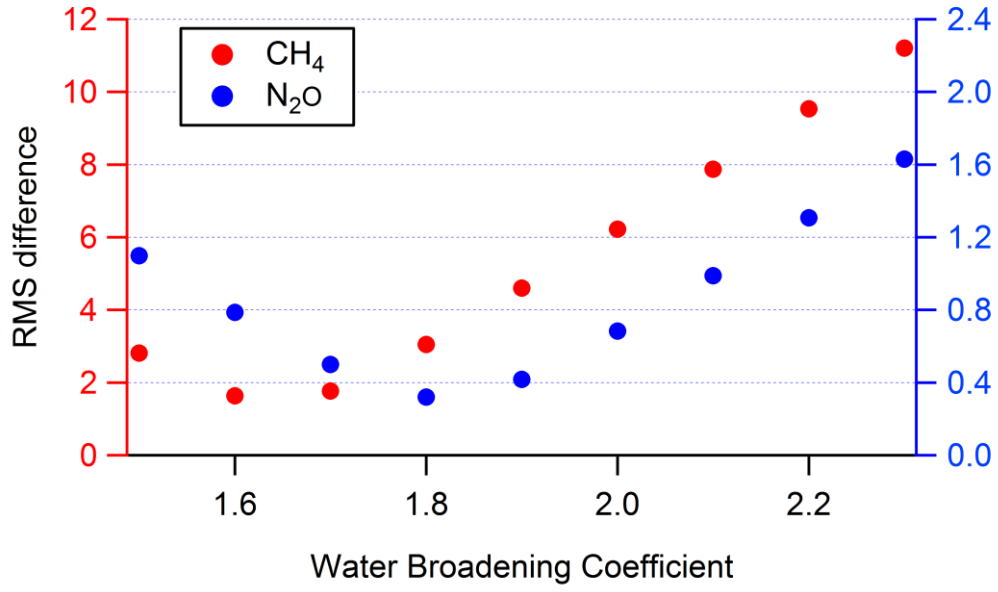


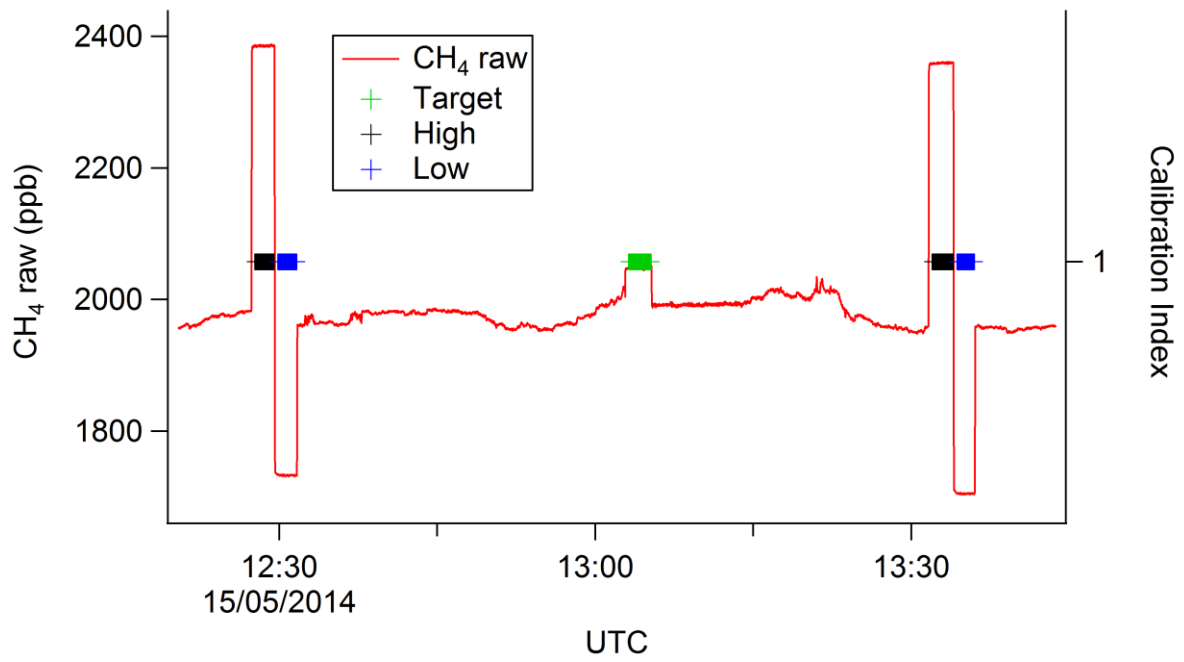
Fig. 1: Schematic showing the QCLAS air sampling and data handling systems. The C.E.P.E. (Calibration, Exhaust, Power and Electronics) unit and the Aerodyne QCL mini monitor enclosures are represented by dashed boxes around the components they contain. The calibration cylinders are labelled "Low", "High", and "Target". The flow rate of the calibration gas is controlled by the MFC (mass flow controller), and the flow rate into the instrument is monitored by the MFM (mass flow meter). The optical components associated with the alignment of the laser beam are not shown.



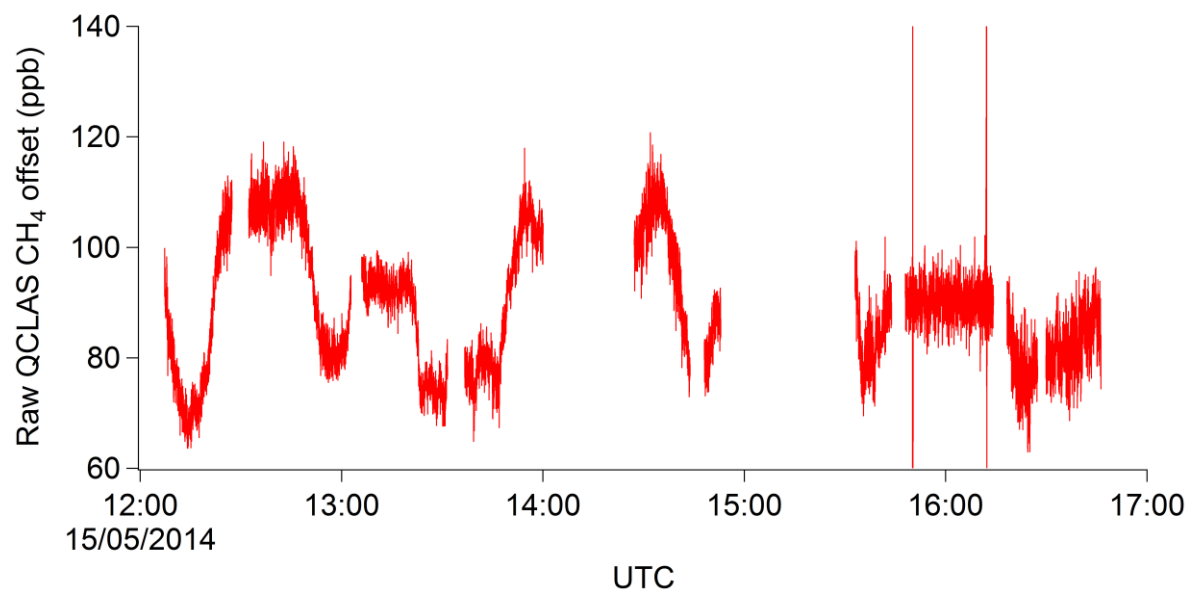
1 **Fig. 2:** Residual error due to the influence of water vapour for the retrieval of a) CH₄ and b)
2 N₂O after applying an empirically derived scale factor to correct the data. Data from four
3 identical experiments is shown; the residuals are calculated as the product of the fractional
4 error for each measurement and the average mole fraction for the dry measurements taken
5 during all four experiments.



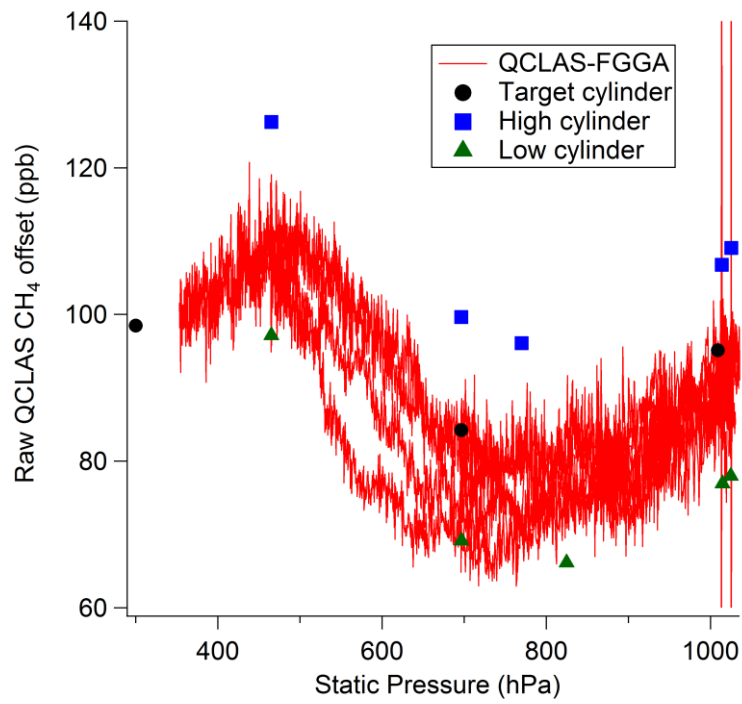
1 **Fig. 3:** RMS (root mean square) difference between the retrieved wet mole fractions and the
2 corresponding dry measurements for CH₄ and N₂O, as a function of water broadening
3 coefficient. These RMS values are determined using data taken over the full experimental
4 range of H₂O mole fraction during all four identical experiments.



1 **Fig. 4:** A selection of raw CH₄ data from flight B848, overlaid with calibration index markers
2 to highlight the hourly calibration cycle. The target cylinder measurement (green markers) is
3 performed approximately mid-way between the high-low span cylinder measurements (black
4 and blue markers respectively) used to calibrate the data to the WMO scale.



1 **Fig. 5:** The offset between the raw QCLAS CH₄ data and the calibrated FGGA data (used
2 here as our reference) during flight B848. Gradients of over 30 ppb in less than 10 minutes
3 can be seen to be present.



1 **Fig. 6:** The offset between the raw QCLAS CH₄ measurements and both the corresponding
2 calibrated FGGA data and the known contents of the target, high and low calibration
3 cylinders during flight B848, shown as a function of static pressure. Although the absolute
4 magnitude of the offset differs for these four different measurements, the same broadly
5 repeatable pattern is exhibited by each of them.

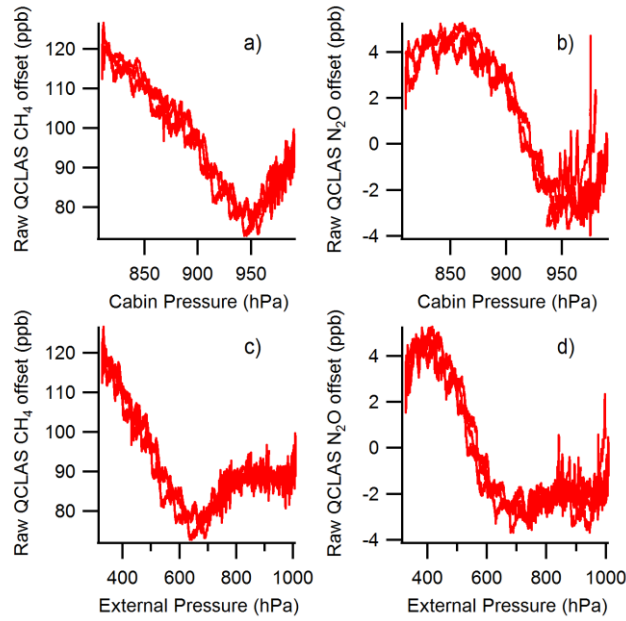
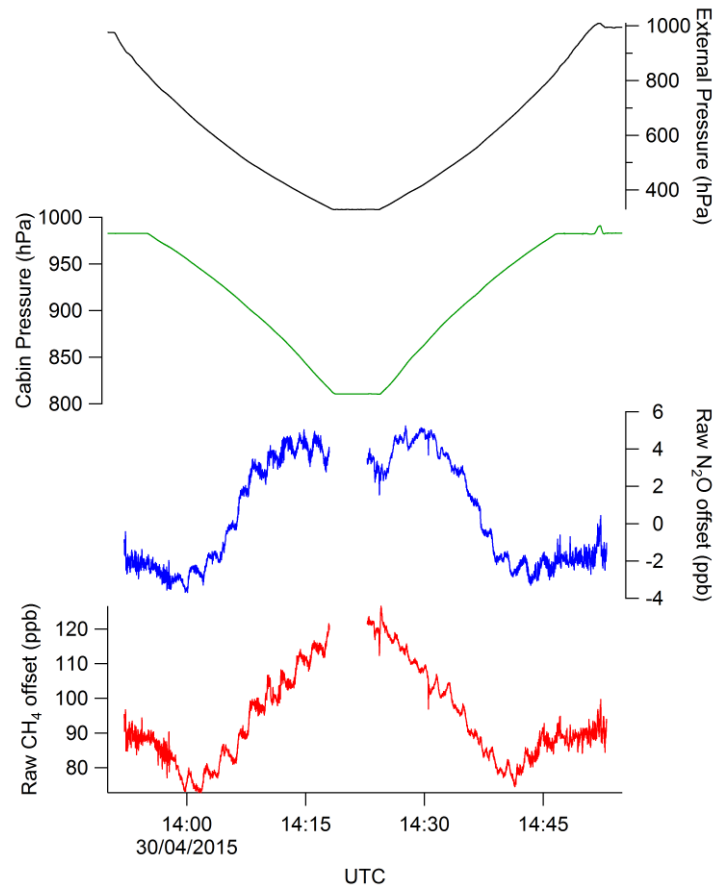


Fig 7: The offset between the raw retrieved QCLAS mole fractions and the known content of a target cylinder, sampled continuously during three separate deep profiles during flight B903. Panels a) and b) shown the offset as a function of the pressure inside the cabin, for CH₄ and N₂O respectively. Panels c) and d) show the offset as a function of external static pressure (also for CH₄ and N₂O respectively).



1 **Fig 8:** Time series from flight B903, showing the offset between the raw retrieved QCLAS
2 mole fractions and the known content of the target cylinder being sampled. Cabin pressure
3 and external static pressure are also shown to illustrate the systematic nature of the offset
4 during two consecutive profiles.

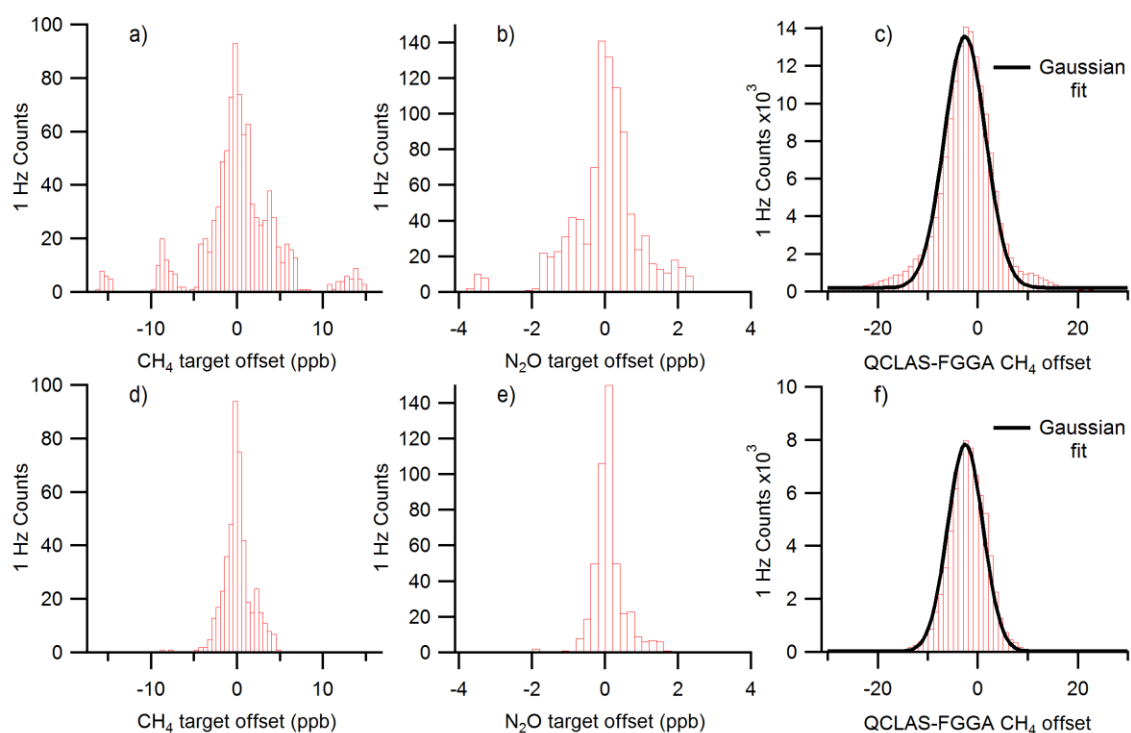
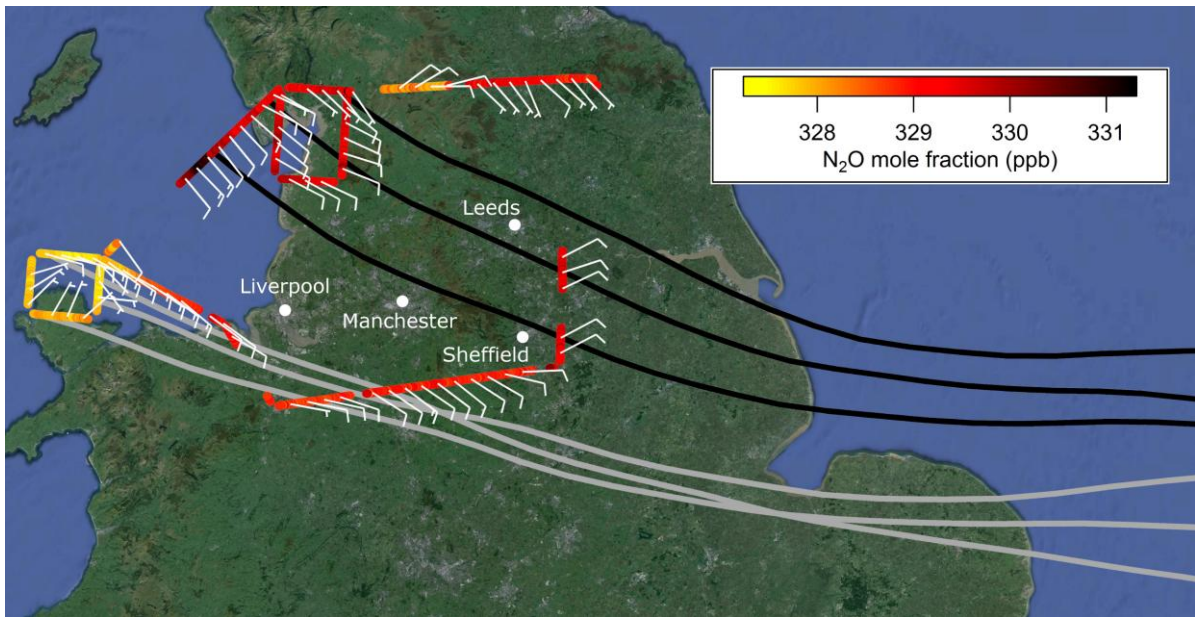


Fig. 9: Histograms showing the offset between the calibrated 1 Hz QCLAS measurements and both the corresponding target cylinder values and the corresponding FGGA sample measurements. Panels a) to c) show histograms for data calibrated using the original method; in comparison panels d) to f) show the corresponding histograms using the pressure-differentiated calibration method. It can be seen here that the pressure-differentiated method results in the removal of many of the outlying target cylinder measurements. In addition, the Gaussian fit to the QCLAS-FGGA CH_4 offset is also improved by the pressure-differentiated calibration method (panel f) relative to the original method (panel c).



1 **Fig. 10:** Aircraft flight track for flight B868, coloured by N₂O mole fraction. Average wind
2 speeds and directions taken over 60 s are shown as a wind barbs (using the convention where
3 each full barb represents a wind speed of 10 knots). Selected HYSPLIT back trajectories are
4 shown for a region of enhanced N₂O (black) and a contrasting region of lower N₂O (grey).
5 Map data: Google, SIO, NOAA, U.S. Navy, NGA, GEBCO, Landsat.